Desalination and Water Treatment
www.deswater.com
doi: 10.1080/19443994.2014.965225

56 (2015) 2937–2947
December

Taylor & Francis
Taylor & Francis Group

Efficient removal of aqueous lead by leached sea nodules residue

N.S. Randhawa*, R.K. Jana

Metal Extraction & Forming Division, CSIR-National Metallurgical Laboratory, Jamshedpur 831007, Jharkhand, India, Tel. +91 657 2345184, +91 9835590339; Fax: +91 657 2345245; email: nsrandhawa@gmail.com (N.S. Randhawa), Tel. +91 657 2345185, +91 9431703888; Fax: +91 657 2345245; email: rkj@nmlindia.org (R.K. Jana)

Received 22 April 2014; Accepted 2 September 2014

ABSTRACT

The sea nodule leaching residue/wastes (generated after recovery of copper, nickel, and cobalt) are hazardous to the environment due to fine nature and heavy metal contents. Here, we demonstrate highly efficient adsorptive remediation of aqueous lead using the residue generated in reduction roast–ammonia leaching of sea nodules. Characterization of leached sea nodule residue (SNR) revealed fine granulometry (d_{50} = 11.4 μm) and high surface area of 66.7 m^2 g^{-1}. Batch adsorption experiments are performed varying temperature, pH of solution, contact time, initial lead concentration, adsorbent dose, etc. to determine lead removal capacity of SNR. Excellent adsorption capacity of lead onto SNR to the tune of 2,500 mg g^{-1} is achieved, which is quite high in comparison with other adsorbents. Kinetics and thermodynamic aspects of adsorption are studied. The pseudo-second-order model is found applicable to the lead removal kinetics. SEM and XRD investigations showed lead adsorbed on the surface of SNR in the form of hexagonal crystalline hydrocerussite.

Keywords: Adsorption; Chemisorption; Heavy metals; Lead; Lead carbonate

1. Introduction

Hydrometallurgical treatment of sea nodule, while recovering copper, nickel, and cobalt metals, generate huge amount (normally 75% of the nodules treated) of leach tailings or residue [1,2]. Sea nodule residues (SNRs) mainly contain oxides/hydroxides of manganese, iron, silicon, calcium, magnesium, aluminum, etc. These residues are viewed as serious threat to the environment if discarded untreated owing to their very fine nature as well as heavy metals contents. To alleviate the environmental problems associated with the handling of these materials, a number of studies have been carried out for its utilization such as production of value-added materials, use as catalyst, adsorbent, etc. [3]. Several value-added materials have been produced using sea nodule leach tailings, which also contribute to improve overall economics of sea nodules processing [4–12]. In addition to this, sea nodules residues contain MnO_2/Mn_2O_3 giving rise to Mn^{3+}–Mn^{4+} couple suitable to catalyze many synthesis and conversion reactions and hence, can be used as catalyst for decomposition of H_2O_2, CO oxidation, esterification of aliphatic acid (selectivity order being formic > acetic > proponoic > n-butyric), oxidation of benzene to phenol, degradation of azo dyes, etc. [13–17]. However, the most interesting and extensively studied application of leached SNR is the adsorptive remediation of heavy metals from wastewater and industrial effluents [18,19]. The fine nature and excellent surface properties of residues generated in

*Corresponding author.

$NH_4OH/(NH_4)_2SO_4$ and $NH_4OH/(NH_4)_2CO_3$ leaching of sea nodules have been successfully exploited for adsorptive remediation of several anionic (PO_4^{2-}, SeO_3^{2-}, $Cr_2O_7^{2-}$, etc.) and cationic (Cd^{2+}, Cu^{2+}, Ni^{2+}, etc.) pollutants from wastewaters [20–27]. However, lead adsorption from aqueous medium has not been studied in details with the leached residue generated in reduction roast–ammonia leaching process of sea nodules. Therefore, present study has been aimed at investigating the sorption properties of residue, generated in the $NH_4OH/(NH_4)_2CO_3$ leaching of sea nodules, for the removal of lead from its aqueous solution. This study is of importance as lead has been found to be responsible for neurotoxicity of central and peripheral nervous systems [28], apart from its presence in drinking water, even in low concentration, may cause diseases such as anemia, hepatitis, nephrine syndrome, etc. [29].

In the present investigation, several parameters have been varied to determine the lead adsorption characteristics of leached sea nodules residue. The lead removal data have been analyzed by widely accepted isotherms and kinetics models. The mechanism governing the lead removal by leached SNR has also been discussed.

2. Materials and methods

2.1. Adsorbent

The SNR is prepared by reduction roasting–ammoniacal leaching of sea nodules. For reduction roasting, 100 mesh grounded sea nodules mixed with fuel oil (12% v/w), heated at 750˚C in a muffle furnace for 1.5 h and collected in a container purged with nitrogen gas to avoid oxidation of roasted product. Roast-reduced sea nodule is then leached with 150 g L^{-1} ammonia solution, with oxygen supply (5 L min^{-1}) at pulp density of 10% and at room temperature for 4 h in a glass reactor with continuous stirring. The leaching slurry is filtered and residue is washed with deionized water to remove the entrapped leach liquor. The washed residue is air-dried for several days for characterization and sorption studies.

2.2. Characterization

Chemical analyses of SNR are determined by combination of conventional wet chemical methods [30] and atomic absorption spectrometer (Perkin Elmer AAnalyst 400). Surface area measurement and pore size analysis are conducted using Quantachrome 4000E surface area analyzer (Nova Instruments, USA). Size analysis of SNR is carried out in Malvern Mastersizer after ultrasonic liberation of particles. Point of zero charge of SNR is determined by acid–base titration method reported by Huang and Ostavic [31]. The microscopic features of the samples are characterized by field emission scanning electron microscope (Nova NanoSEM 430).

2.3. Lead removal studies

The synthetic stock solution of lead (Pb(II)) of 1,000 mg L^{-1} is prepared by dissolving 1.598 g Pb $(NO_3)_2$ in deionized water. Solutions of 0.01 M HNO_3 and 0.01 M NaOH are used for pH adjustment. 0.1 N KNO_3 is used to maintain the ionic strength in all the adsorption experiments. All the chemicals are AR grade and procured from Merck Specialities Pvt. Ltd., Mumbai. Pb(II) removal characteristics of SNR are evaluated through batch kinetics and equilibrium experiments. For kinetic studies, typically, 100 mL of Pb(II) solution at desired concentration with appropriate amounts of SNR in a 250-mL-stoppered conical flask is shaken using a water bath shaker. Samples are withdrawn at certain time interval and remaining Pb (II) in the filtrate is analyzed by atomic absorption spectrometer (PerkinElmer AAanalyst 400). The amount of Pb(II) per gram of the SNR, Q_t (mg g^{-1}) at time t is calculated using Eq. (1).

$$Q_t = \frac{(C_o - C_t)V}{w \times 1,000} \tag{1}$$

where C_o and C_t are the initial Pb(II) concentration (mg L^{-1}) and Pb(II) in solution, respectively, V is the volume of solution in mL, and w the mass of sorbent in gram. The equilibrium adsorption experiments are carried out to investigate the effect of various parameters, such as pH of the Pb(II) solution (3–8), initial Pb (II) concentration (50–1,000 mg L^{-1}), adsorbent dose (25–2,000 mg L^{-1}), and temperature (303–323 K) under fixed equilibration time obtained by kinetics experiments. For the desorption studies, Pb(II)-loaded SNR is transferred into 250-mL-deionized water adjusted to different pH values in the range of 2–7 maintained by 0.1 M HNO_3 and 0.1 M NaOH and shaken for 2 h at 303 K. Thereafter, SNR is filtered/centrifuged and the filtrate is analyzed to determine the concentration of the desorbed metals. Desorption (%) is calculated by Eq. (2).

$$\text{Desorption } (\%) = \frac{\text{Amount of metal ion desorbed}}{\text{Amount of metal ions loaded on SNR}} \times 100 \tag{2}$$

3. Results and discussion

3.1. Characterization of adsorbent

Detailed chemical analyses of SNR are given in Table 1. The manganese, iron, and silicon are the major constituents along with lime, magnesia, and alumina. The particle size distribution (Fig. 1) exhibits fine nature of SNR with mean particle diameter (d_{50}) of 11.4 μm. The pore size distribution of SNR is shown in Fig. 1 depicting wide range of pore width (0.36–106 nm) spanning from micro- (<2 nm), meso- (2–50 nm) to the macro- (>50 nm) pores (Inset Fig. 1). Fig. 2(a) shows the SEM image of SNR, which reveals aggregated bodies of small particles of various sizes. High-resolution SEM image (Fig. 2(b)) of a particle revealed ribbon-like filamentous structure having filaments of ~30–40 nm width. Surface area is determined as 66.7 m^2 g^{-1} in SNR. The pHpzc of SNR, determined by titrimetric procedure, was found to be about 6.5, which is higher than that reported for sea nodules (4.5–4.7) [32,33]. The higher value may be due to lowering of buffering capacity of metal hydr(oxides) due to dehydration in the reduction roasting of manganese nodules. Detailed XRD and IR characterization of SNR carried out previously showed presence of $MnCO_3$, Mn_2SiO_4, and $Mn_2SiO_3(OH)_2{\cdot}H_2O$ phases [27,34]. Absorption bands in SNR at 1,470, 1,070, and 870 cm^{-1} were attributed to the ν(C–O) and δ(OCO) vibrations of the carbonate ion [34]. This indicated the formation of $MnCO_3$ in SNR during the reduction–roasting–leaching cycle for the processing of manganese nodules.

Table 1
Chemical composition of SNR

Element/radical	Mass (%)
Mn	26.11
Fe	10.19
SiO_2	16.44
Al_2O_3	3.54
CaO	0.36
MgO	4.40
Co	0.039
Ni	0.05
Cu	0.13
C	5.59
Moisture	6.18
LOI[a]	17.01

[a]LOI = Loss in weight on ignition.

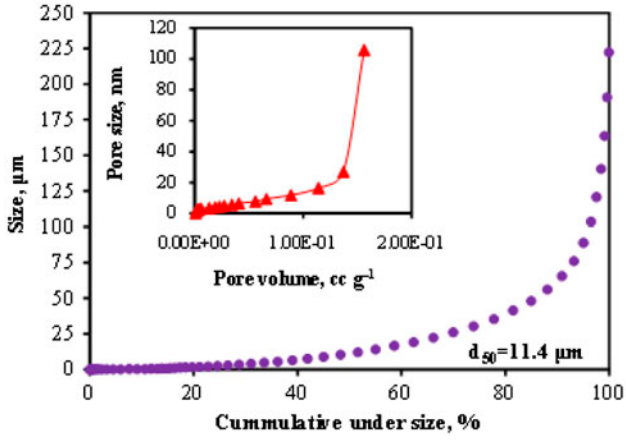

Fig. 1. Particle size distribution in SNR. Inset: Pore size-volume relation.

3.2. Effect of time and initial concentration on adsorption

The time course of Pb(II) adsorption onto SNR, studied with the solutions containing 50, 100, 150, 200, 500, and 1,000 mg L^{-1} Pb(II), SNR dose of 100 mg L^{-1}, pH 5.5 at 303 K, is depicted in Fig. 3. Both the contact time between SNR and Pb(II) and initial concentration of Pb(II) have significant influence on the adsorption of Pb(II) onto SNR. Two types of adsorption patterns are apparent: initial fast adsorption and then slowly reaching equilibrium in all the cases. In case of initial Pb(II) concentrations <500 mg L^{-1}, fast adsorption takes place in the initial 10 min adsorbing more than 50% of the total adsorption value, then reaching slowly to the equilibrium in about 240 min. On the other hand, equilibrium is attained rapidly (within 30 min) in case of initial Pb(II) ≥ 500 mg L^{-1}. The faster adsorption of Pb(II) under identical conditions (pH ~5.5) for initial Pb(II) ≥ 500 mg L^{-1} may be due to better interaction between the adsorbent surface and abundant Pb(II) ions at high initial concentration. As apparent in Fig. 3, initial Pb(II) concentration significantly affects amount of adsorption. Highest adsorption percent of Pb(II) is obtained at the lowest concentration of Pb(II) i.e. 50 mg L^{-1} and adsorption decreases with increasing initial Pb(II) concentration. Hence, SNR can be applied not only to minimize the Pb(II) content in concentrated effluents but also useful for remediation of low Pb(II)-contaminated water to the acceptable limits.

3.3. Effect of pH

The effect of pH on the adsorption of Pb(II) from 100 mg L^{-1} Pb(II), studied by varying the initial pH of solution from 3 to 9, is given in Fig. 4. It is apparent that the uptake of Pb(II) increases with the pH value. The increase in lead uptake can be partly attributed to

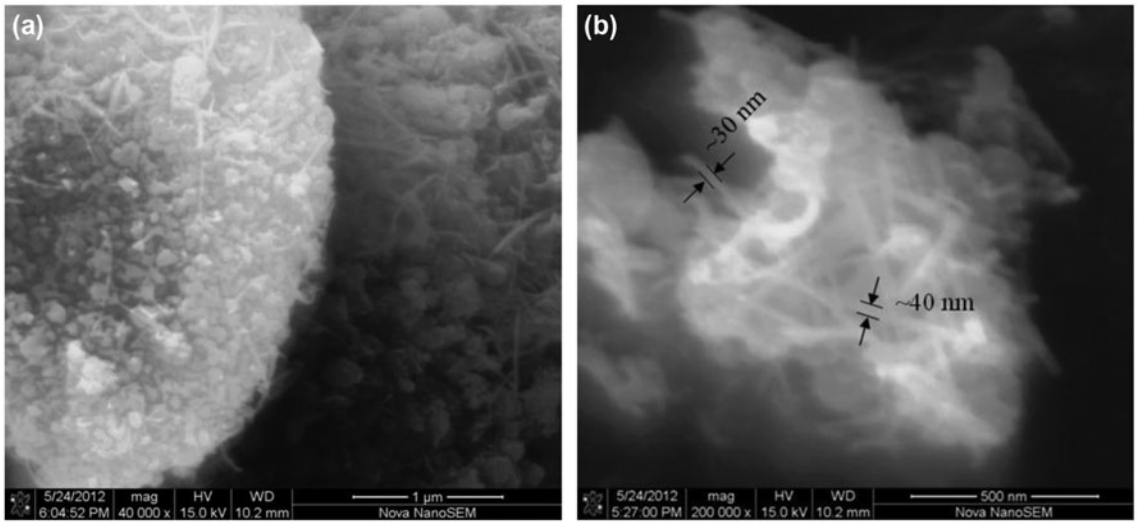

Fig. 2. (a) Low-magnification SEM image and (b) high-magnification SEM image of SNR.

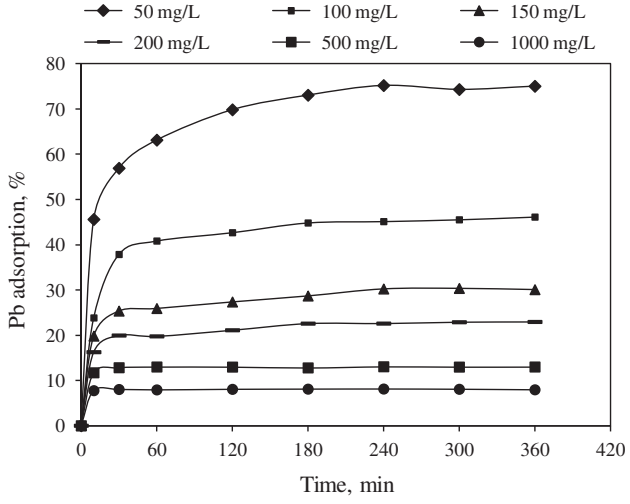

Fig. 3. Effect of time and initial Pb(II) concentration on lead removal with SNR dose of 100 mg L^{-1}, pH 5.5 at 303 K.

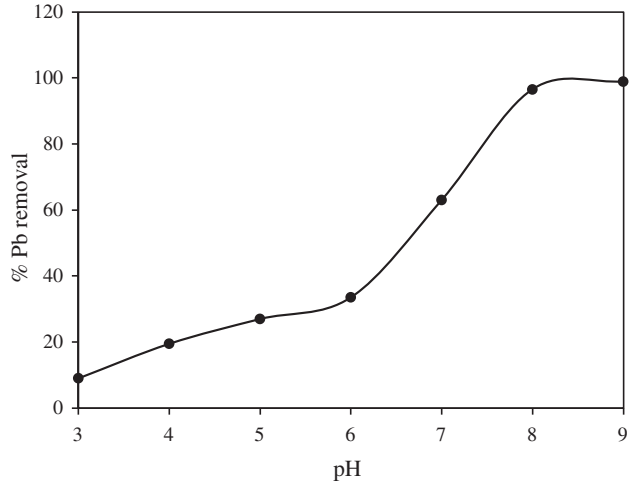

Fig. 4. Effect of solution pH on Pb(II) removal with SNR dose of 100 mg L^{-1}, initial Pb(II) 100 mg L^{-1} at 303 K, and shaking time 240 min.

formation of different hydroxo species with rise of solution pH. The species distribution diagram for Pb (II), as reported in literature, showed that Pb^{2+} is predominant (>95%) species up to pH 6 whereas hydroxo and dihydroxo species are formed after pH 7 [20]. Thus, removal of Pb(II) up to pH 6 is due to adsorption of Pb^{2+} on SNR surface whereas at pH > 6, precipitation of hydroxo anion i.e. $Pb(OH)^+$ as hydroxide over SNR surface plays dominant role in the removal of Pb(II). Another reason may be the abundance of hydronium (H_3O^+) ions in the solution [20,23]. At low pH values, the solution has an excess of H_3O^+ ions and hence, a competition exists between the positively charged H_3O^+ ions and Pb(II) ions for the available negative adsorption sites on the SNR surface. As the pH increases and the concentration of H_3O^+ lowers, more of the positively charged metal ions in solution are adsorbed on the SNR.

3.4. Effect of adsorbent dose

The ratio of amount of adsorbent and aqueous phase i.e. Solid:Liquid is a very important parameter in the adsorption processes, which determines the

optimum adsorbent dose for a certain volume of metal ion solution. Different amounts of SNR were shaken with 100 mL of Pb(II) solution (100 mg L^{-1}) for 240 min at pH 5.5. The results indicated that the lead adsorption increased with increasing SNR addition, as shown in Fig. 5. The positive correlation between adsorbent dose and Pb(II) removal efficiency can be related to the increasing available surface area or binding sites. With the addition of 500 mg L^{-1} SNR, the Pb(II) removal was about 92%. Nearly 100% Pb(II) removal was achieved with addition of 1,000 mg L^{-1} of SNR.

3.5. Adsorption kinetics

The kinetics of sorption is one of the important characteristics for defining the efficiency of an adsorbent. The kinetic studies of Pb(II) sorption on SNR have been carried out with 100 mg L^{-1} Pb(II) solution at pH 5.5 and SNR dose of 100 mg L^{-1} at temperatures of 303, 313, and 323 K. Data from these experiments are fitted into Lagergren kinetic model (Eq. (3)) and pseudo-second-order rate model (Eq. (4)) to estimate the specific rate constant for the adsorption of Pb(II) from aqueous solution [35,36].

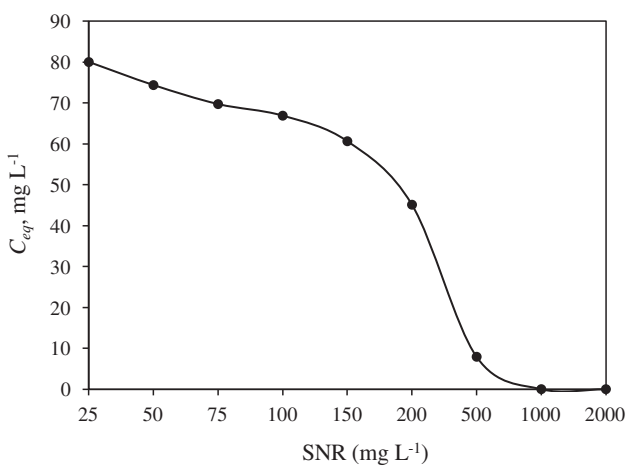

Fig. 5. Effect of SNR dose on Pb(II) removal with initial Pb(II) 100 mg L^{-1}, pH 5.5 at 303 K, and shaking time 240 min; Variations in Pb(II) remaining in the solution at equilibrium after shaking with certain dose of SNR are shown.

$$\ln(q_e - q_t) = \ln q_e - k_1.t \quad (3)$$

$$\frac{t}{q_t} = \frac{1}{k2q_e^2} + \frac{1}{q_e^t} \quad (4)$$

where q_e and q_t refer to the amount of Pb(II) adsorbed per unit weight of adsorbent (mg g^{-1}) at equilibrium and at any time t (min). k_1 and k_2 are the Lagergren kinetic rate constant and pseudo-second-order rate constant, respectively.

$$h_0 = k_2 q_e^2 \quad (5)$$

$$t_{1/2} = 1/k_2 q_e \quad (6)$$

where h_0 is the initial sorption rate (mg g^{-1} min^{-1}) and $t_{1/2}$ = half adsorption time (min).

Straight lines are obtained while fitting the Pb(II) adsorption data into Eqs. (3) and (4), the values of r^2 for Eq. (3) are significantly lower than unity (Table 2). In contrast, higher values of r^2 from Eq. (4) signify that the adsorption of Pb(II) on SNR obeys pseudo-second-order rate kinetics. The rate constant (k_2) changed slightly with temperature but the equilibrium concentration (q_e) changed significantly due to rapid increase in initial rate (h_0) of adsorption from 29.15 to 67.11 mg g^{-1} min when temperature increases from 303 to 323 K. This indicates the effect of temperature on adsorption kinetics is positive and reactions are endothermic in nature. In addition to this, increasing Pb(II) uptake by SNR with the temperature also indicates chemical interaction/bonding during Pb(II) adsorption onto SNR [37].

3.6. Adsorption isotherm studies

The adsorption isotherms have been often used to characterize the equilibrium between the amount of adsorbate that accumulated on the adsorbent and the

Table 2
Lagergren and pseudo-second-order rate constants for adsorption of Pb(II) onto SNR at different temperatures

	Lagergren constants			Pseudo-second-order rate constants			
Temp, K	k_1 (min^{-1})	q_e cal. (mg g^{-1})	r_1^2	k_2 (g mg^{-1} min^{-1})	q_e cal. (mg g^{-1})	h (mg g^{-1} min^{-1})	r_2^2
303	0.010	320.95	0.792	0.00013	476.19	29.15	0.996
313	0.012	316.87	0.919	0.00015	588.24	51.28	0.999
323	0.012	341.17	0.748	0.00017	625.00	67.11	0.998

Table 3
Calculated Langmuir and Freundlich parameters for Pb(II) removal by SNR

	Langmuir isotherm			Freundlich isotherm		
Temp, K	Adsorption maxima q_m (mg g^{-1})	Binding energy constant b (mg $L^{-1})^{-1}$	Regression coefficient r^2	Adsorption capacity K_f (mg g^{-1})	Adsorption intensity $1/n$	Regression coefficient r^2
303	840	0.034	0.999	264	0.173	0.924
313	1,351	0.018	0.999	494	0.141	0.987
323	2,500	0.015	0.999	726	0.158	0.981

Table 4
Maximum loading capacities (q_m) of some high Pb(II) adsorbing materials

Adsorbent	q_m (mg g^{-1})	Reference
Zeolite synthesized from fly ash	524.22	[39]
Hydroxyapatite-Magnetite composites	598.80	[40]
N-methylimidazole modified palygorskite	714.29	[41]
NiO nanoparticles	909.00	[42]
Strontium-hydroapatite nanorods	1,482 ± 137	[43]
Lignin	1,587.15	[44]
Nano-MgO	1,980	[45]
SNR (303 K)	840	Present work
SNR (313 K)	1,351	Present work
SNR (323 K)	2,500	Present work

concentration of the dissolved adsorbate. In the present study, the equilibrium Pb(II) adsorption data were fitted by both the Langmuir (Eq. (7)) and the Freundlich (Eq. (8)) models [20,22,27,38]. The coefficients of these models were computed using linear least-squares fitting.

$$\frac{C_e}{q_e} = \frac{1}{bq_m} + \frac{C_e}{q_m} \tag{7}$$

$$\ln q_e = (1/n)\ln C_e + \ln K_f \tag{8}$$

where q_e is the equilibrium adsorption capacity, mg g^{-1}; C_e is equilibrium liquid phase concentration, mg L^{-1}; q_m is the maximum adsorption capacity, mg g^{-1}; and b is adsorption equilibrium constant, L g^{-1}. The value of b and q_m is obtained from the intercept and slope of the plot between C_e/q_e and C_e. In Eq. (8), K_f and $1/n$ stand for empirical constants related to adsorption capacity and intensity, respectively, and calculated from the intercept and slope of the plot ln q_e and ln C_e. The Langmuir and Freundlich plots for Pb(II) adsorption at 303, 313, and 323 K are drawn to calculated isotherm parameters (Table 3). It is evident that the isotherm data fit better with the Langmuir model (r^2 = 0.999, 0.999, and 0.999) as compared to the Freundlich model (r^2 = 0.924, 0.987, and 0.981) for the adsorption of Pb(II) onto SNR. The increase in the value of q_m with the increasing temperature confirms endothermic nature of Pb(II)–SNR interaction in aqueous solution and the Pb(II) removal

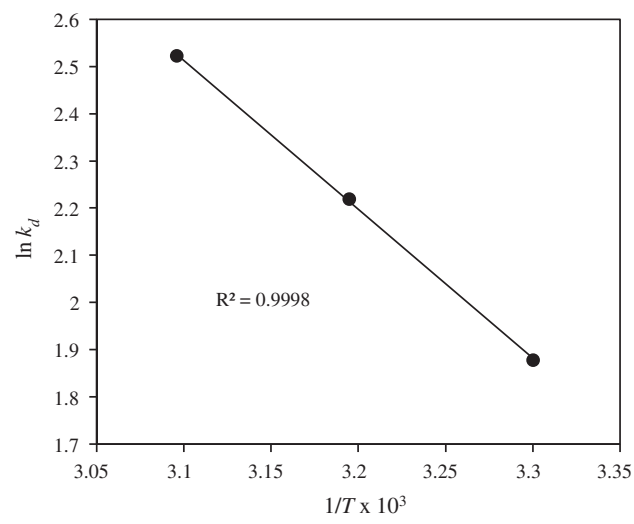

Fig. 6. Determination of thermodynamic parameters.

behavior is analogous to that observed in kinetics studies. The maximum adsorption capacity (q_m) derived from Langmuir isotherm is 840 mg Pb(II)/g SNR at 303 K. This value is found comparable to that of many other high Pb(II) adsorbing materials (Table 4) reported in literature [39–45]. The Pb(II) uptake by SNR enhanced to 1,351 mg Pb(II)/g SNR at 303 K and further to 2,500 mg Pb(II)/g SNR at 323 K. Thus, very high loading capacity coupled with fast kinetics make SNR a potential material for remediation of Pb(II) effluents.

3.7. Thermodynamic studies

The thermodynamic parameters are determined from the thermodynamic equilibrium constant, K_d (or the thermodynamic distribution coefficient), derived from adsorption equilibrium experiments. The standard Gibbs free energy ΔG° (kJ mol^{-1}), standard enthalpy change ΔH° (kJ mol^{-1}), and standard entropy change ΔS° (J mol^{-1} K^{-1}) are calculated using the following equations [38]:

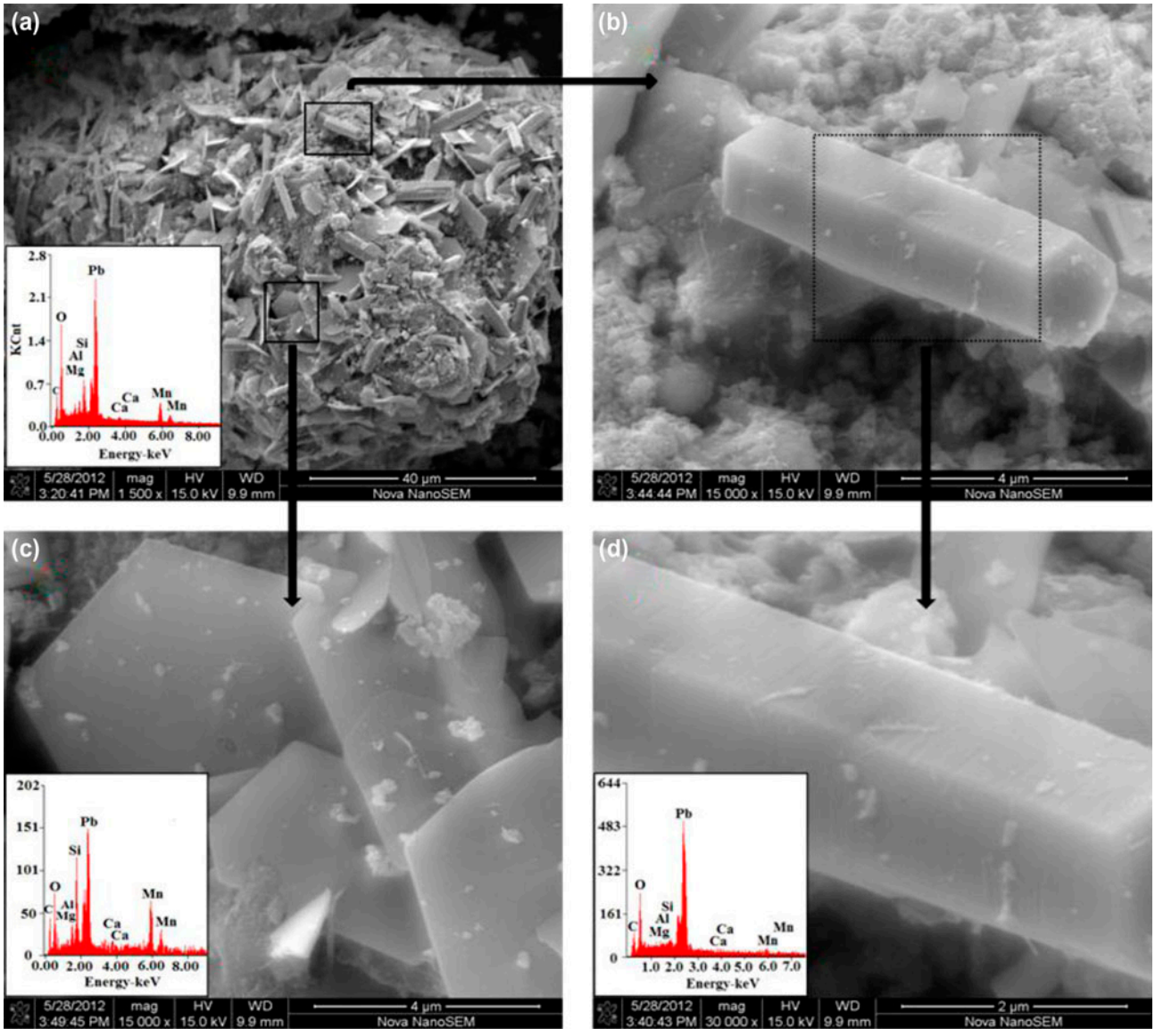

Fig. 7. Scanning electron microscopic examination of Pb(II)-loaded SNR along with bulk EDX spectra (a) A SNR particle fully covered with numerous hexagonal flakes and rod-like structures on the surface, (b) Magnified view of a rod-like formation adhered to the SNR surface, (c) Magnified view of a hexagonal flakes-like formation, and (d) Close view of rod-like formation showing stacked layer pattern.

$$\Delta G^\circ = -RT \ln K_d \quad (9)$$

$$\ln K_d = \frac{\Delta S^\circ}{R} - \frac{\Delta H^\circ}{RT} \quad (10)$$

K_d can be defined as:

$$K_d = \frac{a_s}{a_e} = \frac{\gamma_s C_s}{\gamma_e C_e} \quad (11)$$

where a_s = activity of adsorbed metal ion, a_e = activity of metal ion in solution at equilibrium, γ_s = activity coefficient of adsorbed metal ion, γ_e = activity coefficient of metal ion in equilibrium solution, C_s = metal ion adsorbed on SNR (mg g^{-1}), and C_e = metal ion concentration in solution at equilibrium (mg L^{-1}).

K_d at different temperatures is determined by plotting $\ln(C_s/C_e)$ versus C_s and extrapolating C_s to zero [27,38]. ln K_d thus obtained is plotted against $1/T$ to calculate ΔH° and ΔS° from the slope and intercept, respectively (Fig. 6). Negative values of ΔG° (−4.73, −5.77, and −6.77 kJ mol^{-1} at 303, 313, and 323 K, respectively) indicate spontaneous adsorption and increase in the degree of spontaneity of reaction with the temperature. The positive standard enthalpy (26.23 kJ mol^{-1}) change confirms endothermic nature of Pb(II) adsorption onto SNR. The positive ΔS° (102.18 J mol^{-1} K^{-1}) signify increasing randomness at the solid–solution interface during the adsorption of lead on SNR and reflects the affinity of the SNR toward Pb(II) ion [37,38].

3.8. Mechanism

The uptake of a heavy metal ion (as in the present case) is generally governed by the effect of attraction between adsorbent and adsorbate due to physical or chemical bonding. Numbers of adsorbents are reported to exhibit physical bonding i.e. electrostatic attraction while adsorbing targeted metal ion. However, in case of adsorbents possessing high uptake/removal capacity for certain heavy metal ion, bonding through chemical interaction/exchange, etc. has been prevalent. It is most likely that the exceptionally high Pb(II) removal capacity occurs due to chemical interaction between Pb(II) containing solution and the active groups or metal compounds present on surface of SNR. The SEM image of Pb(II)-loaded SNR is shown in Fig. 7((a)–(d)), showing high abundance of plate-like hexagonal crystalline structures on SNR surface. Apparently, numerous hexagonal rod-like crystals, mostly ~5–10 μm in length and ~2–4 μm diameter, are also present on the surface of SNR. Close examination of a rod-like crystal exhibit hexagonal layers and therefore, seem grown from stacking of hexagonal plate crystals. The chemical composition as determined by bulk EDX of area shown in Fig. 7(a) revealed the major element present on the SNR surface to be Pb (83.86% by mass). Further, EDX of a rod crystal (Fig. 7(c)) shows presence of ~90% Pb along with small amount of manganese, carbon, and Oxygen. The precipitation of Pb(II) as $Pb(OH)_2$ is very unlikely as the pH for precipitation of Pb^{2+} from a 1,000 mg L^{-1} solution is 7.69. The deposited Pb(II) on SNR was further investigated for phase determination by powder XRD of Pb(II)-loaded SNR, shown in Fig. 8. The prominent peaks were identified as lead carbonate hydroxide ($Pb_3(CO_3)_2(OH)_2$) or hydrocerussite (File no. 13-0131) having hexagonal structure. The formations of $PbCO_3$ may take place due to availability of carbonate anions generated by dissociation of $MnCO_3$ of SNR in acidic solution. However, the amount of CO_3^{2-} ions generated by SNR only is not sufficient to remove such high quantity of Pb(II) and likely to be supplied by atmospheric CO_2. To investigate the source of CO_2, few experiments were carried out in the inert atmosphere which showed decreased removal of Pb(II) by 10–30%. This signify that Pb(II) reacted with CO_3^{2-} generated by dissociation of $MnCO_3$ as well as atmospheric CO_2 absorbed in Pb(II) salt solution, to form hydrocerussite. Similar reactions producing hydrocerussite have also been reported for lead pigments in old paintings deteriorated by atmospheric CO_2 as well as metal carbonate solutions [46,47].

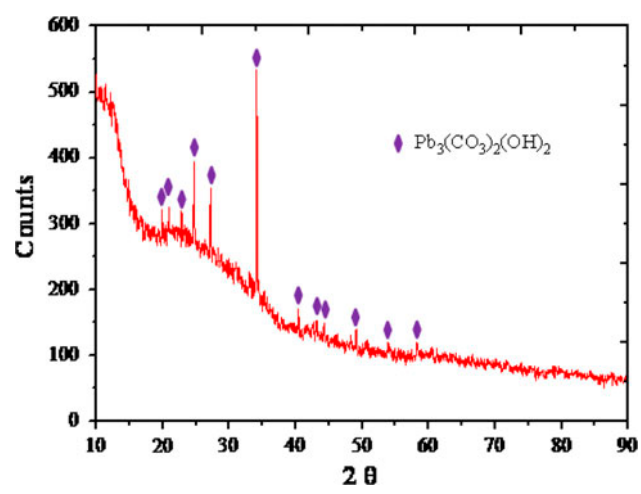

Fig. 8. XRD pattern of Pb(II)-loaded SNR. All prominent peaks are assigned to hydrocerussite phase (File no. 13-0131).

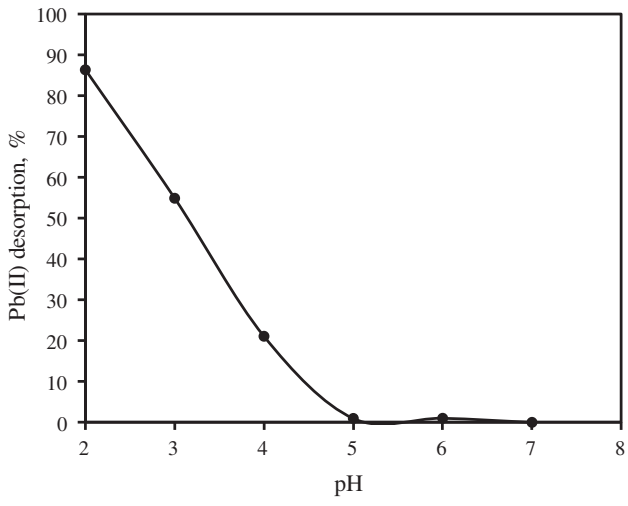

Fig. 9. Desorption of Pb(II) by eluent at different pH.

3.9. Desorption studies

The overall metal removal efficiency of an adsorbent also depends on the metal elution/desorption efficiency of the adsorbed metals. Elution/desorption efficiency was defined in this study, as the ratio of the mass desorbed from the SNR to the mass adsorbed onto the SNR. The deionized water employed as eluent and elution of adsorbed Pb(II) ions was investigated in pH range of 2–7. Like the adsorption, desorption of Pb(II) was also seen to depend upon the pH of the eluent (Fig. 9). It is found that at eluent pH of 2, ~86% Pb(II) could be desorbed/eluted, which decreases with increasing pH of the eluent. Almost nil desorption was seen at eluent pH of 7 or more. Elution studies indicates that Pb(II) adsorption on SNR is not completely reversible and the Pb(II) ions that are strongly adsorbed on the surface are not desorbed.

4. Conclusions

The sea nodules residue (SNR) was characterized and investigated for adsorptive removal of Pb(II) from aqueous solution. Characterization studies showed SNR is amorphous in nature with high surface area (66.7 m^2 g^{-1}). High-magnification SEM revealed filamentous built of SNR particles. The SNR was found highly efficient adsorbent of Pb(II) from aqueous solution. The adsorption equilibrium was found dependent on initial concentration of Pb(II) ion: ~4 h for <500 Pb (II) mg L^{-1} and 30 min for ≥500 mg L^{-1}. Based on regression analysis, pseudo-second-order kinetic was found applicable for the Pb(II) adsorption indicating chemisorption. The Pb(II) uptake data show good fit to Langmuir isotherm than the Freundlich isotherm. The maximum removal capacity of Pb(II) by SNR, determined by Langmuir model, was 840.34 mg g^{-1} at 303 K, which improved to 2,500 mg g^{-1} at 323 K. The formation of lead carbonate hydroxide, confirmed by SEM and XRD studies, during SNR-Pb(II) interaction in the solution is responsible for high Pb(II) removal capacity of SNR. Our study demonstrates environmental-friendly application of SNR in a simple and economical way. The findings of present work may contribute to resolve the hazard associated with lead-contaminated industrial effluents.

References

[1] R. Acharya, M.K. Ghosh, S. Anand, R.P. Das, Leaching of metals from Indian ocean nodules in SO_2–H_2O–H_2SO_4–$(NH_4)_2SO_4$ medium, Hydrometallurgy 53 (1999) 169–175.
[2] R.K. Jana, S. Srikanth, B.D. Pandey, V. Kumar, Premchand, Processing of deep sea manganese nodule at NML for recovery of copper, nickel and cobalt, Met. Mater. Proc. 11 (1999) 133–139.
[3] N.S. Randhawa, Physico-chemical characterization and applications of leached manganese nodule residue generated by reduction roasting—Ammonia leaching, Ph.D Thesis, North Orissa Univeristy, India, 2014.
[4] T.C. Alex, K.M. Godiwalla, S. Kumar, R.K. Jana, A.S. Rao, M. Singh, Studies on extraction of manganese from sea nodule residue as ferro silico manganese, Steel Res. Int. 7 (2006) 147–151.
[5] N.S. Randhawa, R.K. Jana, N.N. Das, Silicomanganese production utilising low grade manganese nodules leaching residue, mineral processing and extractive metallurgy, Trans. Inst. Min. Metall., Sect. C 122 (2013) 6–14.
[6] W. Zhang, C.Y. Cheng, Manganese metallurgy review. Part I: Leaching of ores/secondary materials and recovery of electrolytic/chemical manganese dioxide, Hydrometallurgy 89 (2007) 137–159.
[7] K. Sanjay, S. Anand, R.P. Das, Manganese recovery from ammoniacal leach residues of ocean nodules, Metals Mater. Proc. 11 (1999) 151–160.
[8] J.P. Panda, K. Sanjay, M.K. Ghosh, T. Subbaiah, Electrolytic manganese dioxide (EMD) from manganese cake—A byproduct of nodule process, Proceedings of the eighth ISOPE ocean mining symposium, Chennai, India, 2009, 20–24.
[9] K. Osaki, Y. Hamada, M. Ichijo, Basic study for production of lightweight aggregate from leaching residue of manganese nodule, J. Min. Metall. Inst. Jpn. 103 (1987) 793–798.
[10] J.C. Wiltshire, The use of marine manganese tailings in industrial coatings applications, "Oceans '97", MTS/IEEE, Halifax, Nova Scotia, 1997, pp. 1314–1319.
[11] J.C. Wiltshire John, Beneficial usage of ferromanganese marine mineral tailings, in: K. Narendra Saxena (Ed.), Recent Advances in Marine Science and Technologies, 92, Fifth Pacific Congress on Marine Science and Technology (PACON), Kona, Hawaii, 1992, pp. 405–412.

[12] P.J. Troy, J.C. Wiltshire, Manganese tailings: Useful properties suggest a potential for gas absorbent and ceramic materials, Mar. Georesour. Geotechnol. 16 (1998) 273–281.
[13] L.M. Gandía, M.A. Vicente, A. Gil, Preparation and characterization of manganese oxide catalysts supported on alumina and zirconia-pillared clays, Appl. Catal., A 196 (2000) 281–292.
[14] K.M. Parida, S.S. Dash, S. Mallik, J. Das, Effect of heat treatment on the physico-chemical properties and catalytic activity of manganese nodules leached residue towards decomposition of hydrogen peroxide, J. Colloid Interface Sci. 290 (2005) 431–436.
[15] S.S. Dash, S. Mallik, K.M. Parida, B.K. Mohapatra, Studies on manganese nodule leached residue 4. Physicochemical characterization and catalytic activity of acetic acid treated manganese nodule leached residue, J. Colloid Interface Sci. 294 (2006) 117–121.
[16] K.M. Parida, S.S. Dash, Surface characterization and catalytic evaluation of manganese nodule leached residue toward oxidation of benzene to phenol, J. Colloid Interface Sci. 316 (2007) 541–546.
[17] S.S. Dash, K.M. Parida, Esterification of acetic acid with n-butanol over manganese nodule leached residue, J. Mol. Catal. A 266 (2007) 88–92.
[18] K.M. Parida, S. Mallick, B.K. Mohapatra, V.N. Misra, Studies on manganese-nodule leached residues 1. Physicochemical characterization and its adsorption behavior toward Ni^{2+} in aqueous system, J. Colloid Interface Sci. 277 (2004) 48–54.
[19] K.M. Parida, S. Mallick, S.S. Dash, Studies on manganese nodule leached residues 2. Adsorption of aqueous phosphate on manganese nodule leached residues, J. Colloid Interface Sci. 290 (2005) 22–27.
[20] N.N. Das, R.K. Jana, Adsorption of some bivalent heavy metal ions from aqueous solutions by manganese nodule leached residues, J. Colloid Interface Sci. 293 (2006) 253–262.
[21] S. Mallick, S.S. Dash, K.M. Parida, Adsorption of hexavalent chromium on manganese nodule leached residue obtained from NH_3–SO_2 leaching, J. Colloid Interface Sci. 297 (2006) 419–425.
[22] S.S. Dash, K.M. Parida, Studies on selenite adsorption using manganese nodule leached residues, J. Colloid Interface Sci. 307 (2007) 333–339.
[23] A. Agrawal, K.K. Sahu, Kinetic and isotherm studies of cadmium adsorption on manganese nodule residue, J. Hazard. Mater. 137 (2006) 915–924.
[24] A. Agrawal, K.K. Sahu, B.D. Pandey, A comparative adsorption study of copper on various industrial solid wastes, AIChE J. 50 (2004) 2430–2438.
[25] A. Agrawal, K.K. Sahu, B.D. Pandey, Systematic studies on adsorption of lead on sea nodule residues, J. Colloid Interface Sci. 281 (2005) 291–298.
[26] N.S. Randhawa, N.N. Das, R.K. Jana, Selenite adsorption using leached residues generated by reduction roasting–ammonia leaching of manganese nodules, J. Hazard. Mater. 241–242 (2012) 486–492.
[27] N.S. Randhawa, N.N. Das, R.K. Jana, Adsorptive remediation of Cu(II) and Cd(II) contaminated water using manganese nodule leaching residue, Desalin. Water Treat. 52 (2013) 4197–4211.
[28] J. Hsiang, E. Díaz, Lead and developmental neurotoxicity of the central nervous system, Curr. Neurobiol. 2 (2011) 35–42.
[29] F. Barbosa Jr, J.E. Tanus-Santos, R.F. Gerlach, P.J. Parsons, A critical review of biomarkers used for monitoring human exposure to lead: Advantages, limitations, and future needs, Environ. Health Perspect. 113 (2005) 1669–1674.
[30] A.I. Vogel, A text book of quantitative inorganic analysis, fourth ed., Longmans, London, 1978.
[31] C.P. Huang, F.G. Ostavic, Removal of Cd(II) by activated carbon adsorption, J. Environ. Eng. Div. 104 (1978) 863–878.
[32] S. Bhattacharjee, S. Chakrabarty, S. Maity, S. Kar, P. Thakur, G. Bhattacharyya, Removal of lead from contaminated water bodies using sea nodule as an adsorbent, Water Res. 37 (2003) 3954–3966.
[33] K.M. Parida, P.K. Satapathy, N. Das, Studies on Indian ocean manganese nodules: IV. Adsorption of some bivalent heavy metal ions onto ferromanganese nodules, J. Colloid Interface Sci. 181 (1996) 456–462.
[34] R.K. Behera, P.K. Satapathy, N.S. Randhawa, N.N. Das, Adsorptive removal of phosphate ions using leached sea nodule residue generated by the reduction-roasting ammoniacal leaching process, Adsorpt. Sci. Technol. 28 (2010) 611–628.
[35] Y.S. Ho, Citation review of Lagergren kinetic rate equation on adsorption reactions, Scientometrics 59 (2004) 171–177.
[36] Y.S. HO, Review of second-order models for adsorption systems, J. Hazard. Mater. 136 (2006) 681–689.
[37] V.C. Srivastava, I.D. Mall, I.M. Mishra, Characterization of mesoporous rice husk ash (RHA) and adsorption kinetics of metal ions from aqueous solution onto RHA, J. Hazard. Mater. 134 (2006) 257–267.
[38] H.K. Boparai, M. Joseph, D.M. O'Carroll, Kinetics and thermodynamics of cadmium ion removal by adsorption onto nano zerovalent iron particles, J. Hazard. Mater. 186 (2011) 458–465.
[39] W. Qiu, Y. Zheng, Removal of lead, copper, nickel, cobalt, and zinc from water by a cancrinite-type zeolite synthesized from fly ash, Chem. Eng. J. 145 (2009) 483–488.
[40] L. Dong, Z. Zhu, Y. Qiu, J. Zhao, Removal of lead from aqueous solution by hydroxyapatite/magnetite composite adsorbent, Chem. Eng. J. 165 (2010) 827–834.
[41] Y. Chang, H. Liu, F. Zha, H. Chen., X. Ren, Z. Lei, Adsorption of Pb(II) by N-methylimidazole modified palygorskite, Chem. Eng. J. 167 (2011) 183–189.
[42] T. Sheela, Y.A. Nayaka, Kinetics and thermodynamics of cadmium and lead ions adsorption on NiO nanoparticles, Chem. Eng. J. 191 (2012) 123–131.
[43] F. Zhang, Z. Zhao, R. Tan, W. Xu, G. Jiang, W. Song, Efficient and selective immobilization of Pb^{2+} in highly acidic wastewater using strontium hydroxyapatite nanorods, Chem. Eng. J. 203 (2012) 110–114.
[44] S.K. Srivastava, A.K. Singh, A. Sharma, Studies on the uptake of lead and zinc by lignin obtained from black liquor—A paper industry waste material, Environ. Technol. 15 (1994) 353–361.

[45] C.Y. Cao, J. Qu, F. Wei, H. Liu, W.G. Song, Superb adsorption capacity and mechanism of flowerlike manganesium oxide nanostructures for lead and cadmium ions, ACS Appl. Mater. Interfaces 4 (2012) 4243–4287.
[46] E. Kotulanová, P. Bezdička, D. Hradil, J. Hradilová, S. Švarcová, T. Grygar, Degradation of lead-based pigments by salt solutions, J. Cult. Herit. 10 (2009) 367–378.
[47] E. Kotulanová, J. Schweigstillová, S. Švarcová, D. Hradil, P. Bezdička, T. Grygar, Wall painting damage by salts: Causes and mechanisms, Acta Res. Rep. 18 (2009) 27–31.